Comparison of various models for piezoelectric receivers in wireless acoustic power transfer

Ahmed Allam, Karim Sabra, and Alper Erturk

G. W. Woodruff School of Mechanical Engineering, Georgia Institute of Technology, Atlanta, GA USA 30332 USA

ABSTRACT

Piezoelectric transduction has lately been employed in wireless acoustic power transfer (APT) for powering electronic components that cannot be accessed easily, such as deep-implanted medical devices. Typically, the axial (or thickness) vibration mode of piezoelectric materials is used to generate acoustic waves that propagate through a medium, which are then converted back into electricity and delivered to an electrical load at the receiver end. The piezoelectric receiver can have various aspect ratios (length/diameter) in a given APT application. This work aims to develop and compare various models, such as the classical theory, Rayleigh's theory, and Bishop's theory, as well as finite-element model simulations, for different aspect ratios with an emphasis on those with comparable dimensions. Following analytical modeling and numerical simulation efforts, both in air and fluid loaded impedance frequency response functions are compared to report the valid aspect ratio ranges of the respective theories and their limitations, along with comparisons against experiments.

Keywords: Wireless power transfer, piezoelectric, acoustics

1. INTRODUCTION

Acoustic power transfer (APT) provides the means for powering wireless devices located in remote, hazardous or inaccessible locations. A typical APT system consists of a transmitter (TX) connected to power source, and a receiver (RX) which is integrated into the electronic device to be powered. The transmitter converts the source electrical power into acoustic waves which carries the energy across the medium. The receiver then captures these waves and converts it back to electrical power. This is usually done through a signal conditioning circuit. Acoustic power transfer applications include powering biomedical implants, 1,2 transmitting energy through metallic walls and powering wireless sensors along industrial pipelines 4 among others.

In an APT system (Figure 1), piezoelectric transducers are used to convert electrical power into acoustic waves and vice versa. Krimholtz, Leedom and Matthae (KLM)⁵ and Mason equivalent circuit models are usually used to model TX and RX; however, both models are only developed for the thickness expander plate (thin infinite plate assumption) and thus can only be used for extreme aspect ratios β , where $\beta = \frac{h}{a}$ is the ratio of the transducer thickness h to its height a. For many of the suggested APT systems, size and frequency constraints lead to transducers with moderate aspect ratios for which Mason and KLM models are inadequate. In this work, we derive several continuum analytical models from basic principles to approximate the response of a thickness mode piezoelectric transducer. The validity range of these models is investigated by comparing their numerical predictions to the values obtained using finite element method (FEM) simulations as well as experimental measurements of the impedance of 33-mode PZT transducers. The impedance is measured and simulated both in air and with fluid loading.

Send correspondence to A.E.: alper.erturk@me.gatech.edu

Active and Passive Smart Structures and Integrated Systems XII, edited by Alper Erturk, Proc. of SPIE Vol. 10967, 109670S · © 2019 SPIE · CCC code: 0277-786X/19/\$18 · doi: 10.1117/12.2515377

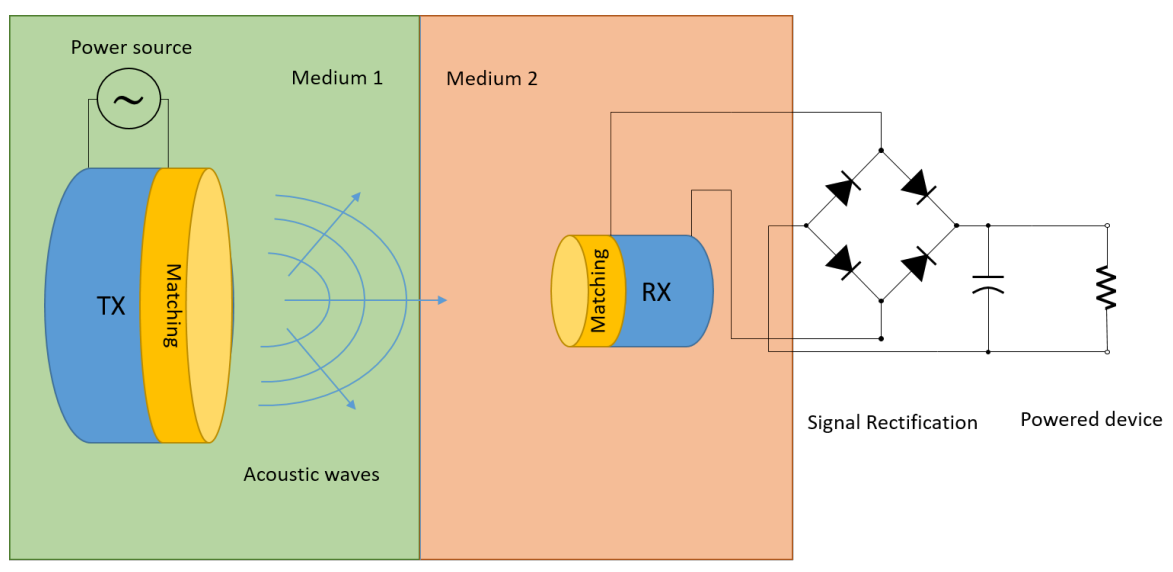


Figure 1. Schematic of a typical wireless APT system.

2. RECEIVER DYNAMICS

A continuum of piezoelectric material is governed by the piezoelectric constitutive equations which are given in their stress-charge form by:

$$T = \mathbf{C}^E S - \mathbf{e}^T E \tag{1}$$

$$D = \mathbf{e}S + \epsilon^S E,\tag{2}$$

where T and S are the stress and engineering strain vectors, E and D are the electric field and electric displacement vectors respectively, \mathbf{C}^E is the compliance matrix, ϵ^s is the electric permittivity matrix and \mathbf{e} is the piezoelectric coupling matrix.

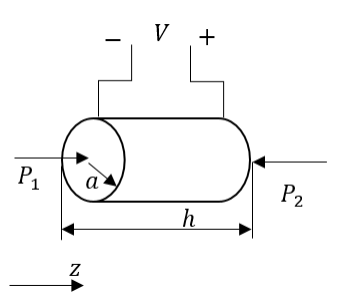


Figure 2. Schematic of a piezoelectric rod transducer.

A cylindrical piezoelectric transducer with height h and radius a is considered (Figure 2). The transducer is polarized in the longitudinal (z) direction and thin metallic electrodes are deposited on its circular faces. The lateral components of the electric field and thus the electric displacement vanishes; therefore, Equations (1) and

(2) can be simplified to:

$$T_1 = C_{11}S_1 + C_{12}S_2 + C_{13}S_3 - e_{31}E_3 \tag{3}$$

$$T_2 = C_{12}S_1 + C_{22}S_2 + C_{13}S_3 - e_{31}E_3 \tag{4}$$

$$T_3 = C_{13}S_1 + C_{13}S_2 + C_{33}S_3 - e_{33}E_3 \tag{5}$$

$$T_4 = C_{44}S_4 (6)$$

$$T_5 = C_{44}S_5 (7)$$

$$T_6 = \frac{C_{11} - C_{12}}{2} S_6 \tag{8}$$

$$D_3 = e_{31}S_1 + e_{31}S_2 + e_{33}S_3 + \epsilon_{33}E_3. (9)$$

In the cylindrical coordinates (r, θ, z) , the engineering strain is related to the displacement fields by:⁶

$$S_{1} = \frac{du_{r}}{dr}, \quad S_{2} = \frac{1}{r} \left(\frac{du_{\theta}}{d\theta} + u_{r} \right), \quad S_{3} = \frac{du_{z}}{dz}, \quad S_{4} = \frac{1}{r} \frac{du_{z}}{d\theta} + \frac{du_{\theta}}{dz},$$

$$S_{5} = \frac{du_{r}}{dz} + \frac{du_{z}}{dr}, \quad S_{6} = \frac{1}{r} \left(\frac{du_{r}}{d\theta} - u_{\theta} \right) + \frac{du_{\theta}}{dr},$$

$$(10)$$

where u_r, u_θ and u_z are the displacements in r, θ and z directions respectively. The modified Hamilton's principle for a piezoelectric volume is given by:^{7,8}

$$\int_{t_1}^{t_2} \delta\left(\overline{T} - U + W_e + W_{nc}\right) dt = 0, \tag{11}$$

where \overline{T} is the total kinetic energy of the rod, U is the total potential (elastic) energy of the rod, W_e is the electric energy stored in the rod and W_{nc} is the work due to the non-conservative forces acting on the rod including the external mechanical and electrical forces, given by:

$$\overline{T} = \frac{1}{2} \int_{V} \rho \left(\dot{u}_r^2 + \dot{u}_\theta^2 + \dot{u}_z^2 \right) dV \tag{12}$$

$$U = \frac{1}{2} \int_{V} (\sigma_1 s_1 + \sigma_2 s_2 + \sigma_3 s_3 + \sigma_4 s_4 + \sigma_5 s_5 + \sigma_6 s_6) dV$$
 (13)

$$W_e = \frac{1}{2} \int_{V} E_3 D_3 dV \tag{14}$$

$$W_{nc} = \int_{S} \left(\bar{t}_r u_r + \bar{t}_\theta u_\theta + \bar{t}_z u_z - \bar{q}\phi \right) dA, \tag{15}$$

where ρ is the mass density, V is the volume, S is the external surface of the transducer, \overline{t} is the external traction acting on the surface of the transducer, \overline{q} is the external surface charge density, and ϕ is the electric voltage applied to the surface.

2.1 Classical thin rod model

For a symmetric thin rod, the lateral stresses and shear stresses are assumed to be very small i.e:

$$T_1 = T_2 = T_4 = T_5 = T_6 = 0 (16)$$

The longitudinal displacement u_z is assumed to have the form:

$$u_z = u\left(z, t\right),\tag{17}$$

and the electric potential $\phi(z,t)$ is related to the electric field E_3 by:

$$E_3 = -\frac{d\phi}{dz}. (18)$$

Substituting by Equations (16-18) into Equations(10) and Equations(3-9) into Equation (11), taking the variation of the integral with respect to u(z,t) and $\phi(z,t)$ and performing integration by parts yields the electromechanical governing equations:

$$\rho u^{(0,2)}(z,t) - \overline{C}u^{(2,0)}(z,t) + \overline{e}\phi^{(2,0)}(z,t) = 0$$
(19)

$$\bar{e}u^{(2,0)}(z,t) - \bar{\epsilon}\phi^{(2,0)}(z,t) = 0,$$
 (20)

and the boundary conditions:

$$-A_{p}\left(\overline{C}u^{(1,0)}(z,t) + \overline{e}\phi^{(1,0)}(z,t)\right) + P_{1,2}(t) = 0\Big|_{z=0,h}$$
(21)

$$A_{p}\left(\overline{e}u^{(1,0)}(z,t) - \overline{\epsilon}\phi^{(1,0)}(z,t)\right) - Q(t) = 0\Big|_{z=0,h}$$
(22)

where the superscript (m, n) indicates the mth derivative with respect to z and the nth derivative with respect to t, and:

$$\overline{C} = C_{33} - \frac{2C_{13}^2}{C_{11} + C_{12}}, \overline{e} = e_{33} - \frac{2C_{13}e_{31}}{C_{11} + C_{12}},
\overline{\epsilon} = \epsilon_{33} + \frac{2e_{31}^2}{C_{11} + C_{12}}$$
(23)

where A_p is the cross-sectional area of the transducer. Equations (21) and ((22)) describe the mechanical and electrical boundary conditions respectively. Assuming harmonic plane-wave solutions of the form

$$u(z,t) = A_u e^{i(\omega t - kz)} + B_u e^{i(\omega t + kz)}$$
(24)

where $k = \frac{\omega}{c}$ is the wavenumber, ω is the angular frequency of the wave, $c = \sqrt{\frac{\overline{C}^D}{\rho}}$ is the speed of sound in the transducer and A_u, B_u are the complex amplitudes of the forward and backward traveling displacement waves. The transducer will be considered as a 3-port element as shown in Figure 3. The boundary conditions given by Equations (21,22) can be used to estimate a scattering matrix which relates incident and reflected waves at each port (both electrical and mechanical waves). The transducer scattering matrix $\bf S$ is given by:

$$\begin{bmatrix} B_1 \\ B_2 \\ B_v \end{bmatrix} = \mathbf{S} \begin{bmatrix} A_1 \\ A_2 \\ A_v \end{bmatrix} = \begin{bmatrix} S_{11} & S_{12} & S_{13} \\ S_{21} & S_{22} & S_{23} \\ S_{31} & S_{32} & S_{33} \end{bmatrix} \begin{bmatrix} A_1 \\ A_2 \\ A_v \end{bmatrix}, \tag{25}$$

where A_1, B_1, A_2, B_2 are the incident and reflected pressure waves on faces 1 and 2 and A_v, B_v are the incident and reflected voltage waves on the electrodes as shown in Figure 3(b).

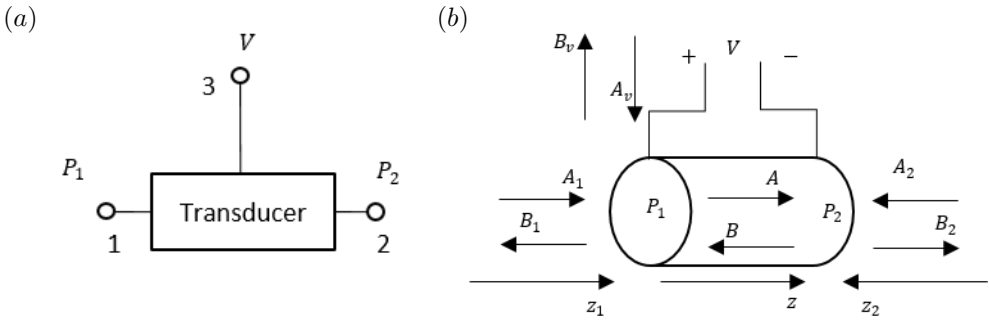


Figure 3. (a) Three-port element representation and (b) schematic of a piezoelectric transducer with arrows indicating incident and reflected voltage and pressure waves

Assuming propagating waves, the boundary conditions could be rearranged into matrix form:

$$\mathbf{M}_1 \begin{bmatrix} B_1 & B_2 & B_v & A_u & B_u \end{bmatrix}^T = \mathbf{M}_2 \begin{bmatrix} A_1 & A_2 & A_v \end{bmatrix}$$
 (26)

where M_1 and M_2 are (5x5) and (5x3) system matrices. The scattering matrix is then:

$$\mathbf{S} = \mathbf{M}_3 \mathbf{M}_1^{-1} \mathbf{M}_2 \tag{27}$$

where

$$\mathbf{M}_3 = \begin{bmatrix} 1 & 0 & 0 & 0 & 0 \\ 0 & 1 & 0 & 0 & 0 \\ 0 & 0 & 1 & 0 & 0 \end{bmatrix} \tag{28}$$

2.2 Rayleigh model

The Rayleigh approach, also known as the Rayleigh-Love rod theory, includes the effect of lateral inertia by assuming the displacement fields of an axisymmetric thin rod to have the form:

$$u_z = u(z,t)$$

 $u_r = -\nu r u^{(1,0)}(z,t)$
 $u_\theta = 0$ (29)

where $\nu = C_{13}/(C_{11} + C_{12})$ is Poisson's ratio. The model can be used for transducers with lower aspect ratios up to the limit where radial and shear modes start affecting the response of the transducer. Following the same procedure as the thin rod, we derive the electromechanical governing equations:

$$A_{p}\rho u^{(0,2)}(z,t) = A_{p}\overline{C}u^{(2,0)}(z,t) + A_{p}\overline{e}\phi^{(2,0)}(z,t) + I_{p}\nu^{2}\rho u^{(2,2)}(z,t)$$
(30)

$$\overline{e}u^{(2,0)}(z,t) - \epsilon_{33}\phi^{(2,0)}(z,t) = 0, \tag{31}$$

and the boundary conditions:

$$-A_{p}\overline{C}u^{(1,0)}(z,t) - A_{p}\overline{e}\phi^{(1,0)}(z,t) - I_{p}\nu^{2}\rho u^{(1,2)}(z,t) + P_{1,2}(t) = 0|_{z=0,h}$$
(32)

$$A_{p}\left(\overline{e}u^{(1,0)}(z,t) - \epsilon_{33}\phi^{(1,0)}(z,t)\right) - Q(t) = 0|_{z=0,h}$$
(33)

where I_p is the polar moment of inertia of the rod:

$$I_p = \int_S r^2 dS \tag{34}$$

As with the thin rod case, the electrical and mechanical interface matching conditions can be used to construct the scattering matrix using Equation (27).

2.3 Bishop model

The Bishop rod theory, also known as the Rayleigh-Bishop, accounts for the coupling between longitudinal and radial displacements inside the rod through the shear elastic modulus (C_{44}). Following the same energy approach yields:

$$A_{p}\rho u^{(0,2)}\left(z,t\right) + C_{44}I_{p}\gamma^{2}u^{(4,0)}\left(z,t\right) = A_{p}\overline{C}u^{(2,0)}\left(z,t\right) + A_{p}\overline{e}\phi^{(2,0)}\left(z,t\right) + I_{p}\nu^{2}\rho u^{(2,2)}\left(z,t\right) \tag{35}$$

$$\overline{e}u^{(2,0)}(z,t) - \epsilon_{33}\phi^{(2,0)}(z,t) = 0,$$
(36)

and boundary conditions:

$$-A_{p}\overline{C}u^{(1,0)}(z,t) - A_{p}\overline{e}\phi^{(1,0)}(z,t) + I_{p}\nu^{2}\left(C_{44}u^{(3,0)}(z,t) - \rho u^{(1,2)}(z,t)\right) + P_{1,2}(t) = 0\bigg|_{z=0,h}$$
(37)

$$u^{(2,0)}(z,t) = 0\Big|_{z=0,h} \tag{38}$$

$$A_{p}\left(\overline{e}u^{(1,0)}(z,t) - \epsilon_{33}\phi^{(1,0)}(z,t)\right) - Q(t) = 0\Big|_{z=0,h}$$
(39)

As with the Rayleigh case, the electrical and mechanical interface matching conditions can be used to construct the scattering matrix. The main difference is the additional two mechanical boundary equations introduced in Equations (37,38).

3. RESULTS FOR DIFFERENT ASPECT RATIOS

The accuracy of the analytical model predictions is investigated through comparisons to FEM simulations and experimental measurements of the impedance of different PZT transducers under different loading conditions.

3.1 Numerical model

COMSOL Multiphysics^{®9} was used to construct a 2D-axisymmetric model for a cylindrical piezoelectric transducer. A coupled multi-physics model was constructed to model the behavior of the transducer both in vacuum (Air) and submerged in a fluid (water/oil). The electrical impedance of two cylindrical piezoelectric transducers in both in air and oil were measured using a Solartron SI 1260 impedance analyzer. The dimensions of the first transducer were 10 mm diameter and 25 mm height ($\beta = 5$) to represent a moderately thick rod, while the second one had a 14 mm diameter and 10 mm height ($\beta = 1.7$) representing a cylinder of comparable diameter to height value. Both transducers are made of a modified PZT-5A piezoelectric material with a thin layer of sliver electrodes on each circular face.

3.2 In vacuo electromechanical impedance

Figure 4 shows the amplitude of the impedance in air for both of the investigated transducers. The results obtained experimentally is compared to that obtained using the numerical and the different analytical models. The boundary conditions for the transducer in air resembles a free-free boundary in the analytical and FEM models. To obtain the impedance of the transducer using FEM, a voltage source was connected between the two electrodes of the transducer, and natural free boundary conditions were applied to all surfaces of the transducer.

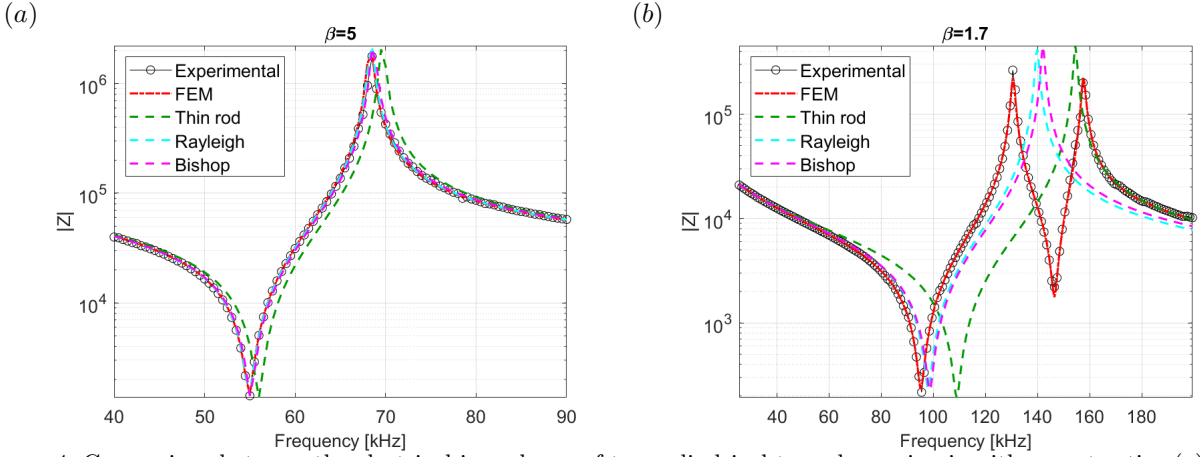


Figure 4. Comparison between the electrical impedance of two cylindrical transducers in air with aspect ratios (a) $\beta = 5$ and (b) $\beta = 1.7$. The experimental results are compared to those estimated numerically using the FEM and analytically using thin rod, Rayleigh, and Bishop rod theories.

For the $\beta=5$ transducer (Figure 4a), excellent agreement between the experimental, FEM, Rayleigh and bishop models is observed. The thin rod model for this aspect ratio predicts a 2% higher resonance and anti-resonance frequencies for the free transducer. This indicates that the effects of lateral inertia cannot be neglected for this aspect ratio or lower. The accuracy of both Rayleigh and Bishop models is quite similar, with the more simplified Rayleigh model actually producing slightly more accurate results. This behavior is expected for relatively thin rods, since the Rayleigh model tends to better approximate the exact solution of a continuous cylinder at low frequencies (around the 1st mode of the transducer) while it deviates more quickly for higher frequencies.⁶

For the $\beta = 1.7$ transducer (Figure 4b), only the FEM model matches the experimental impedance, while all the analytical models predict higher values for the first thickness resonance (95 kHz) of the transducer. While the thin rod approximation is clearly not appropriate anymore for this aspect ratio, the Rayleigh and Bishop

model predictions only deviate 3% higher than the exact value. The analytical models failed to capture the 1st radial resonance appearing around (146 kHz). This is because all the investigated theories are pure longitudinal theories, and even though the effects of lateral inertia are accounted for in Rayleigh and Bishop models, lateral modes are still not considered in the kinematics of the problem. For the considered aspect ratio, the lateral and longitudinal modes appear at close frequency ranges, such that more complicated coupled modes start to appear.

3.3 Fluid loaded electromechanical impedance

The impedance of the investigated transducers was also measured while the transducers were submerged in soybean oil ($c = 1465 \,\mathrm{m/s}$ and $\rho = 917 \,\mathrm{kg/m^3}$). To capture the effect of fluid loading, the fluid domain around the transducer was included in the simulation and coupled acoustic structure boundaries were applied between the structural and acoustic domains. For the presented analytical models, the presence of the transducer in a fluid domain can only be accounted for using the unbaffled acoustic radiation impedance (Z_{rad}) present on the two acoustic ports. The value of this impedance represents the effect of the fluid on the two circular faces of the transducer.

The radiation impedance appearing on a circular radiator depends mainly on the relation between the wavenumber inside the fluid (k_m) and the radius of the radiator (a). Simple approximate formulas for the unbaffled radiation impedance only exist for the cases where $k_m a \ll 1$ and $k_m a \gg 1$. For the investigated aspect ratios $k_m a$ is 1.14and 2.9 for $\beta = 5$ and $\beta = 1.7$ respectively, which does not allow the use of such approximations. In this case, the radiation impedance becomes very complicated to be estimated analytically, since the pressure field generated by the transducer is not only dependent on the front circular face of the transducer, but the interactions between the fields generated by the lateral as well as the back face of the transducer. Neglecting the interactions between the back and lateral sides of the transducer, the radiation impedance can be estimated from Ref.¹⁰ The resulting formula is complicated, and so usually normalized plots¹¹ are used directly instead of the formula itself.

While accounting for fluid loading for the faces of the transducer can be approximated using the unbaffled impedance, doing so for the lateral side of the transducer when it is fully submerged is not possible for the analytical methods presented here. This is because all the analytical rod models used assume that the lateral stress is equal to zero for their derivation.

The effect of fluid loading on the electromechanical impedance of both transducers is shown in Figure 5. For both transducers, good agreement between the experimental and FEM results is observed. Due to the reasons mentioned before, the analytical models tend to account for less fluid loading effects. The models predict higher/sharper resonance values when the value of β is small enough for lateral stresses to be substantial, but not too small that the lateral surface area becomes negligible. Generally, for $\beta > 10$ or $\beta < 0.1$, the lateral stresses are very small and could be safely ignored. For the $\beta = 1.7$ transducer (Figure 5b), the estimated values of the electromechanical impedance appears noisy near the resonance of the transducer. This is attributed to reflections from boundaries of the container which has a finite size compared to an infinite medium assumption. These reflections are more prominent near the 1st resonance of the transducer since it becomes a more efficient radiator. The reflection effects are less obvious in the $\beta = 5$ radiator since it is a less directional acoustic radiator compared to the $\beta = 1.7$ radiator.

4. CONCLUSIONS

Several continuum analytical models for estimating the 33-mode dynamics of a piezoelectric transducer with a cylindrical shape have been investigated with a focus on the effect of aspect ratio. The selection of the appropriate model depends on the aspect ratio of the transducer (β). When the radius of the transducer is very small (i.e ($\beta > 10$), the thin rod analytical model can be used to predict the surface velocity of the transducer around its resonance frequency. However, transducers with comparable aspect ratios are commonly used, especially as receivers. The Rayleigh and Bishop rod models can be used to predict the surface velocity of rod transducers with ($\beta > 3$) around their resonance frequency given that the lateral sides of the transducer are not fluid loaded. When the diameter of the transducer is comparable to its length ($\beta \cong 2$), the longitudinal and lateral motion/modes are strongly coupled, and they become difficult to model analytically. The thin plate thickness model used with

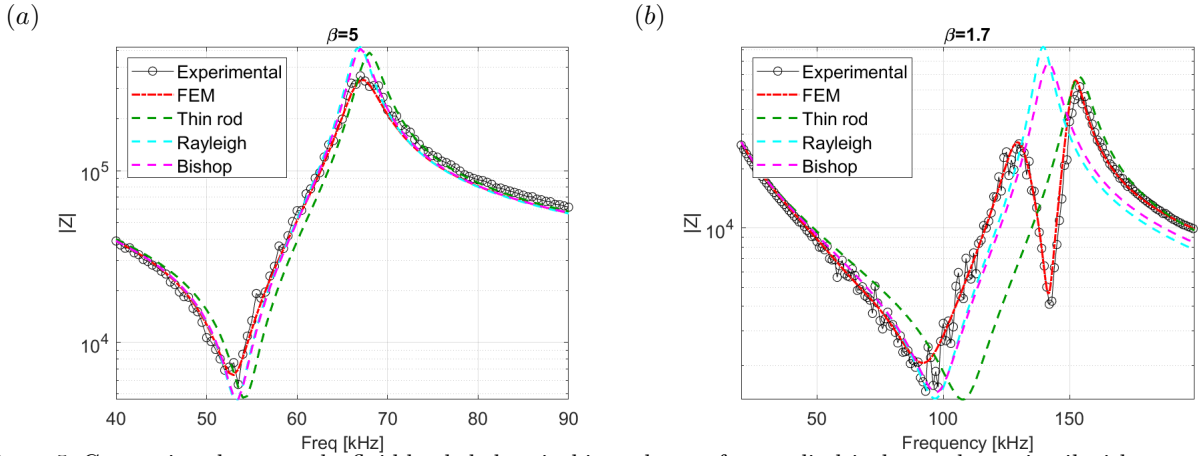


Figure 5. Comparison between the fluid loaded electrical impedance of two cylindrical transducers in oil with aspect ratios (a) β =5 and (b) β =1.7. The results obtained experimentally are compared to those estimated numerically using the FEM and analytically using thin rod, Rayleigh and Bishop rod theories.

equivalent circuit techniques (e.g. KLM, Mason) can only be used when the radius of the transducer is very large compared to its thickness ($\beta < 0.1$).

ACKNOWLEDGMENTS

This work was supported by the National Science Foundation CMMI grant 1727951.

REFERENCES

- [1] Ozeri, S. and Shmilovitz, D., "Ultrasonic transcutaneous energy transfer for powering implanted devices," *Ultrasonics* **50**, 556–566 (May 2010).
- [2] Song, S. H., Kim, A., and Ziaie, B., "Omnidirectional Ultrasonic Powering for Millimeter-Scale Implantable Devices," *IEEE Transactions on Biomedical Engineering* **62**, 2717–2723 (Nov. 2015).
- [3] Leung, H. F., Willis, B. J., and Hu, A. P., "Wireless electric power transfer based on Acoustic Energy through conductive media," in [2014 9th IEEE Conference on Industrial Electronics and Applications], 1555–1560 (June 2014).
- [4] Kiziroglou, M. E., Boyle, D. E., Wright, S. W., and Yeatman, E. M., "Acoustic energy transmission in cast iron pipelines," *J. Phys.: Conf. Ser.* **660**(1), 012095 (2015).
- [5] Krimholtz, R., Leedom, D. A., and Matthaei, G. L., "New equivalent circuits for elementary piezoelectric transducers," *Electronics Letters* **6**, 398–399 (June 1970).
- [6] Shatalov, M., Marais, J., Fedotov, I., and Tenkam, M. J., "Longitudinal vibration of isotropic solid rods: from classical to modern theories," InTech Open (Dec. 2011).
- [7] Tiersten, H. F., "Hamilton's principle for linear piezoelectric media," *Proceedings of the IEEE* **55**, 1523–1524 (Aug. 1967).
- [8] Dym, C. L. and Shames, I. H., [Solid mechanics: a variational approach], Springer Science+Business Media, New York, augmented edition ed. (2013). OCLC: ocn816164751.
- [9] "COMSOL Multiphysics Reference Manual, version 5.4."
- [10] Nimura, T. and Watanabe, Y., "Effect of a Finite Circular Baffle Board on Acoustic Radiation," *The Journal of the Acoustical Society of America* **25**, 76–80 (Jan. 1953).
- [11] Beranek, L. L. and Mellow, T. J., [Acoustics: sound fields and transducers], Academic Press, and imprint of Elsevier, Amsterdam, first edition ed. (2012).